micron

Micron 32 (2001) 363–370

Some efficient methods to correct confocal images for easy interpretation

P.S. Umesh Adiga*, B.B. Chaudhuri[1]

Wellcome Trust Centre for Human Genetics, University of Oxford, Oxford, OX3 7BN, UK

Received 27 April 1999; revised 6 April 2000; accepted 14 April 2000

Abstract

In this paper we have explained some efficient methods to correct artefacts in confocal laser beam scanning microscope (CLSM) images. The main aim is to enhance object features such that they become clearly visible for interactive evaluation and to reduce the overall noise so that the automatic segmentation and feature measurement can be done easily. A simple automatic-thresholding technique, and a straightforward method to restore the light intensity along the depth of the image stack are proposed. Another problem associated with the CLSM is the non-isotropic resolution. We have presented an interpolation technique based on XOR contouring and morphing to virtually insert the image slices in the image stack for improving the axial resolution. This interpolation technique has the merits of both contour- and intensity-based interpolations. Results of application of these methods on CLSM data are shown.

Keywords: Photobleaching; Intensity; Restoration; Noise; Interpolation; Morphing

1. Introduction

The advent of confocal laser scanning microscope (CLSM) in the late 1980s has opened up a new chapter in visualizing biological specimens. Confocal microscopes are capable of delivering a high resolution, three-dimensional (3D) image of biological specimens. Confocal microscopy has prompted many developments in multi-dimensional imaging (Pawley, 1995). Three-dimensional confocal images are a stack of optical sections (2D images) giving a depth view. Such a stack of optical sections is normally contaminated with artefacts and noise due to improper specimen preparation, imaging instruments and non-linear optics. Redesigning the optics and instrument electronics to obtain better-quality images is an expensive and challenging task with limitations to achieving optimality. Application of image-processing techniques to reduce artefacts and correct some of the non-linearity present in the images has been explored for quite some time now. In this paper we present a few techniques to correct the artefacts in CLSM images and to improve axial resolution. The technique to make the image voxel virtually isotropic is based on interpolation by XOR contouring and morphing. Simple but useful techniques to separate background from foreground and to reduce the light attenuation along the depth of the image stack are also discussed.

Section 2 of the paper gives a brief idea of the material and the type of images used in our experiments. Section 3 gives some of the pre-processing steps useful for reducing the artefacts. Section 4 explains the process of interpolation by XOR contouring and morphing while Section 5 gives a brief discussion about the utility of image processing for feature measurement and automation of decision making.

2. The source material

We have tested image-processing techniques on two kinds of data sets obtained using a confocal microscope. The first type consists of routinely processed, formalin-fixed and paraffin-embedded tissue specimens from radical prostatectomies of patients with prostate carcinoma (Aubele et al., 1996). In the second type of data sets we have used samples of industrial sludge showing the filamentous structure of different kinds of bacterias. The samples were taken from industrial sludge treatment plants. The data sets were provided by the Institute of Pathology, GSF, Munich, Germany.

The multi-spectral volumetric image is obtained using a confocal microscope. Fluorescence images are scanned using a confocal laser scanning microscope Zeiss LSM410, lens Zeiss PNF 100×, 1.3, zoom = 2, realised by scanning unit. A lateral pixel size of 0.25 μm is obtained. Excitation laser lines are selected based on the

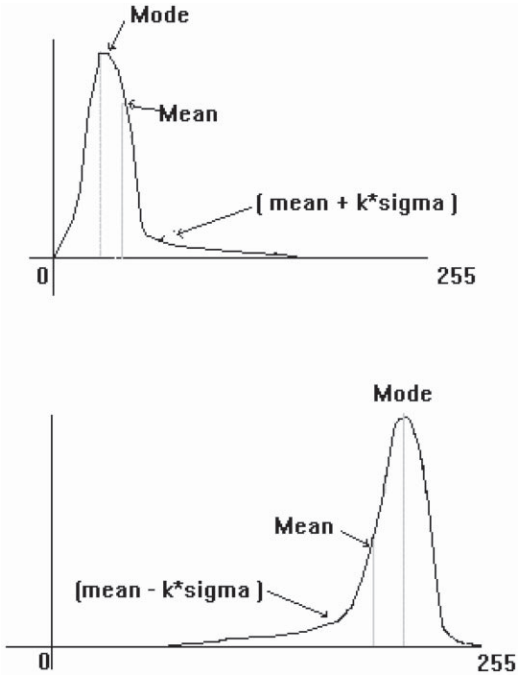

Fig. 1. Diagrammatic representation of threshold selection.

fluorochromes used. For propidium iodide (PI) that is used as DNA counter-stain and FITC labelled signals, both are excited by the Argon line at 488 nm.

3. Pre-processing

One of the common problems with confocal image interpretation is the presence of uneven background and bleed-through from other colour channels. Global thresholding fails to deliver the required separation of background from foreground. Techniques like rank levelling, fitting a background function, etc. (Jain, 1995; Russ, 1995) may deliver acceptable results but they are computation intensive.

For images with a distinct background, it is possible to select the threshold from the grey level histogram using the mode method, i.e. by choosing the grey level that corresponds to a valley position in the histogram as the threshold value. We have observed that the histograms of many confocal image data sets exhibit a unimodal property. Hence the valley may not be found explicitly in the histogram of the images. In such cases it is often possible to define a good threshold at the *shoulder* of a histogram. We have used the empirical formula,

$$\tau = (\mu \pm k\sigma)$$

where σ is the standard deviation of the grey value and k is a data-driven value determined iteratively using the following simple algorithm. Let N_k be the number of voxels in the foreground when the image is thresholded at some value of k.

for $i = 0$ do
$\Delta = N_i - N_{(i+1)}$
if $\Delta \leq (10/100)(N_i)$ then $k = i$
else $i = i + 1$ and repeat till the above condition holds.

We use $\tau = (\mu + k\sigma)$ when the mode point of the histogram lies close to the minimum grey value in the image and $\tau = (\mu - k\sigma)$ when the mode point lies close to the maximum grey value in the image. This is diagrammatically shown in Fig. 1. The above formula gives reasonably good separation of foreground from background. Fig. 2 shows a few image slices of a confocal image stack after background separation. Size and shape filters are used to remove the artefacts of abnormal sizes and shapes.

The uneven illumination along the depth of a specimen results in a spatial variation of light intensity in the image. Degradation of image intensity along the depth of the specimen can be approximately modelled as a first-order decay process and hence computationally corrected. In confocal images, variation in image intensity is not just due to photobleaching of the specimen. Problems with the optical system, as well as the opacity of the specimen, also contribute to the process. When we plot the average image intensity of each image slice against the depth of the stack, we have observed that the illumination degradation is not linear. Rigaut et al. (1992) have proposed a mathematical correction method based on the log–logistic equation: $I_z = I_0/\{1 + (z/Z)^{\xi}\}$ where I_z is the mean field intensity, I_0 is the theoretical value of I_z when $z \rightarrow 0$, the constant Z represents the value of z at which the detected fluorescence intensity (I_z) is half that of I_0 and the constant ξ depends upon the shape of the curve of I_z against z. Parameter estimations were made using the linear form $\log\{(I_0 - I_z)/I_z\} = \xi \log(z) - \xi \log(Z)$, $\forall z \neq 0$ with $\log\{(I_0 - I_z)/I_z\}$ against $\log(z)$. The parameters were estimated by computer iteration over I_0 (above the highest observed value of I_z), until the highest linear-regression correlation coefficient is found.

We have implemented a simple method for restoration of intensity of the foreground voxels by comparing them with the highest-intensity image slice in the stack. Let I_i be the image slice having maximum average image intensity, i.e. $I_i = \max\{I_1, I_2, \ldots, I_n\}$, where $I_1, I_2, \ldots, I_n$ are the intensities of 1, 2,…, nth image slice in the stack. We consider the image slice i as the standard image slice and increase the average image intensity of the remaining image slices in the stack to be on par with the average intensity of the image slice i.

Let the sensitivity α of a pixel with respect to its neighbourhood, defined as the ratio of the sum of the differences of voxel intensities in the neighbourhood to the maximum of voxel intensities in the neighbourhood, i.e.

$$\alpha = \frac{\left(\sum_{p=1}^{N} (I - I_p)\right)}{\max\{I_p\}} \qquad \text{for all } p \in W$$

where W is a 3×3 neighbourhood and N is the total number

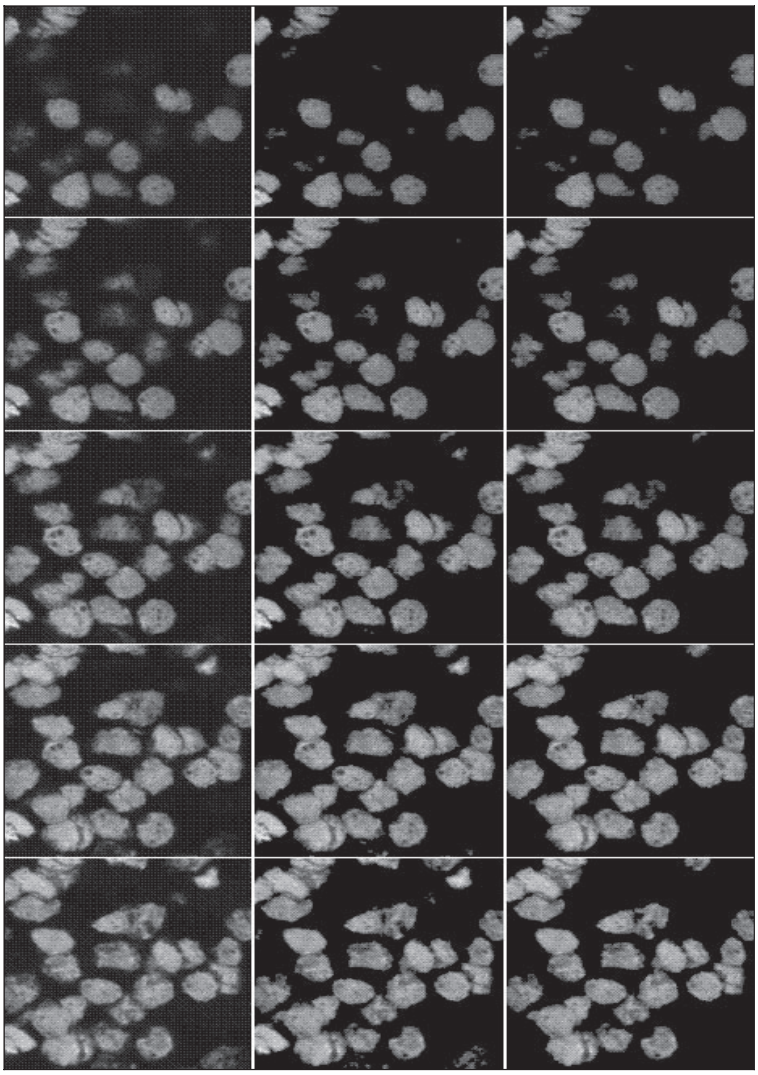

(a) (b) (c)

Fig. 2. Result of window slicing and size filtering: (a) original image slice; (b) after window slicing; and (c) after size filtering.

of pixels in W. Simple restoration of the image intensity by increasing the mean intensity of the image slices results in a decrease of α. An ideal algorithm should find the maximum light restoration with minimum loss of voxel sensitivity. This is an optimization problem and a trade-off should be reached depending upon the application.

The first few image slices may have one or two cell signatures with a relatively high grey value, while the middle and/or last image slices may have very few cell signatures, as can be seen in Fig. 2(a). Thus increasing the average image intensity of the whole image slice increases the background intensity too, which is undesirable. We have considered only those voxels that belong to a particular region of interest where the intensity compensation is necessary while avoiding the other regions such as the background. The necessary separation of foreground and background is obtained as explained earlier.

Let the mean intensities of the image slices 1, 2,…, n, in the image stack be $\bar{I}_1, \bar{I}_2, \ldots, \bar{I}_n$. The variation in the average image intensity of the foreground pixels is plotted in Fig. 3. The maximum average intensity of foreground of the image slices is considered as a reference image slice, i.e. if $\bar{I}_i$ is the average intensity of the reference image slice, such that $\bar{\imath}_i \geq \bar{\imath}_j$ for all j, then image slice i is considered as the reference image slice and $\bar{\imath}_i$ as the standard image intensity value. The difference between the average intensity of image slices with the reference image slice is calculated. Let $\beta_k = |\bar{\imath}_i - \bar{\imath}_k|$ be the difference of average intensity of the foreground in the kth image slice and the reference image slice i. Then for the kth image slice the grey level of each pixel of the foreground is enhanced by a factor $c\beta_{\mathrm{k}}$, i.e. if I(x,y,k) is the intensity of the voxel at I(x,y,k) then the enhanced intensity is given as $I(x, y, k) = I(x, y, k) + c\beta_k$ where c is an experimentally chosen constant. Ideally c should be 1. As stated earlier, this simple addition of the average value to the image intensity results in the loss of voxel sensitivity. A

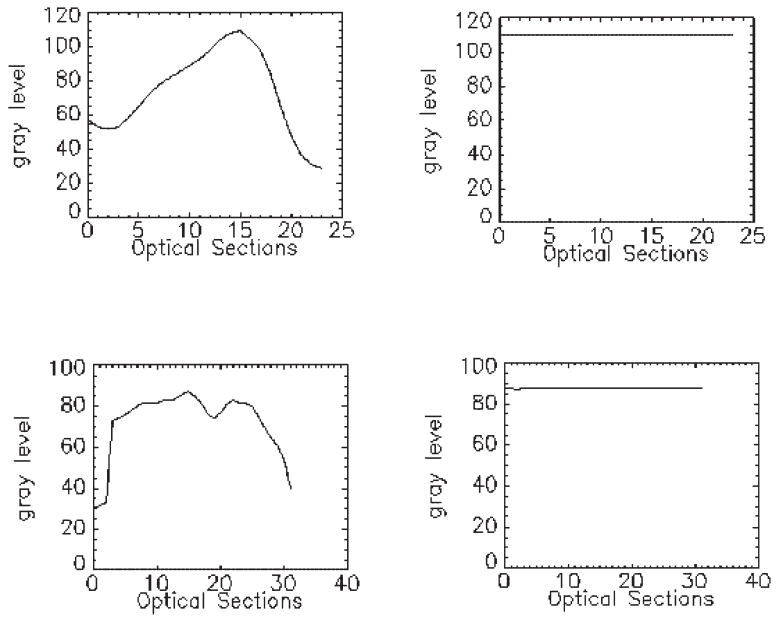

(a) (b)

Fig. 3. Graph showing the average image intensity of the foreground against depth for two specimen images: (a) before restoration; and (b) after restoration.

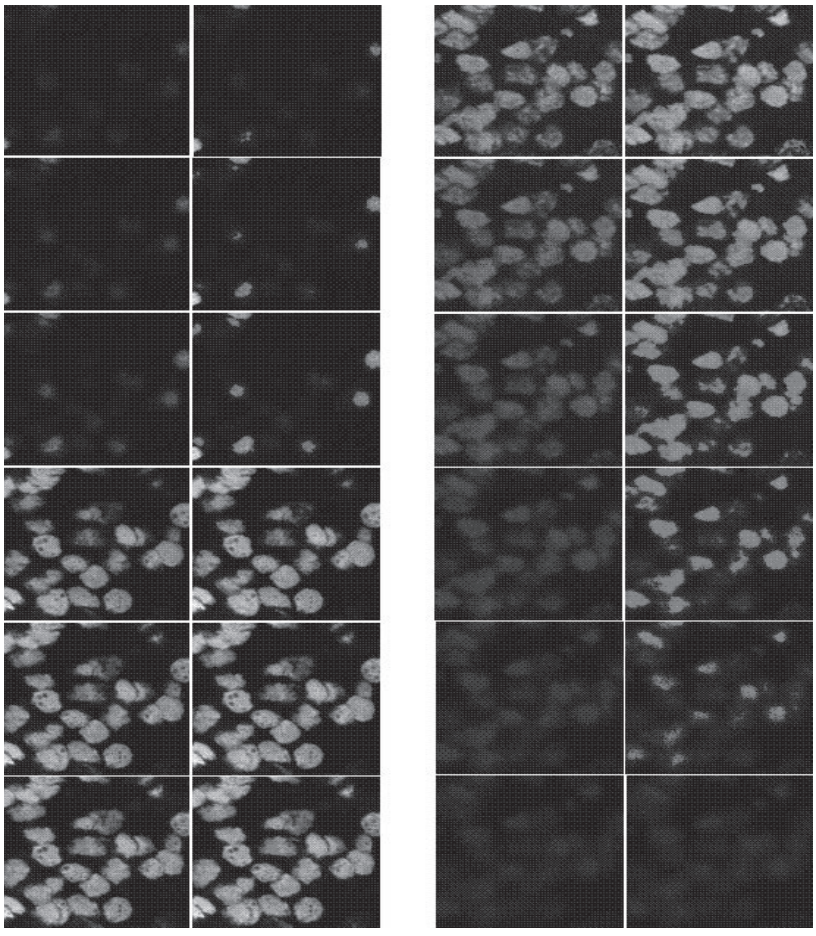

(a) (b) (a) (b)

Fig. 4. Image slices 1, 2, 3, 11,12, 13, 18, 19, 20, 21, 22, 23, of a stack of 24 image slices: (a) before restoration; and (b) after restoration.

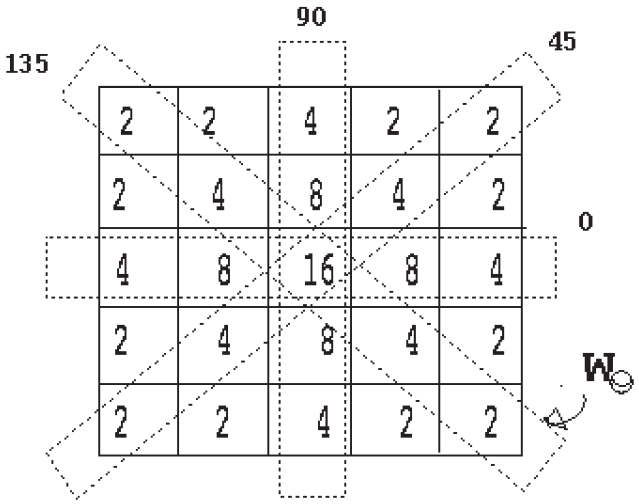

Fig. 5. Directional Gaussian-weighted filter.

trade-off optimizing the requirements of light intensity and loss of sensitivity is useful. This trade-off is also imaging- and application-dependent. As the confocal microscopy images do not give clear details of the intra-cellular structures and our interest is limited to measuring the quantitative features of cells and the tissue, we have ignored the voxel sensitivity issue. Fig. 4 shows the result of intensity restoration on a sequence of image slices.

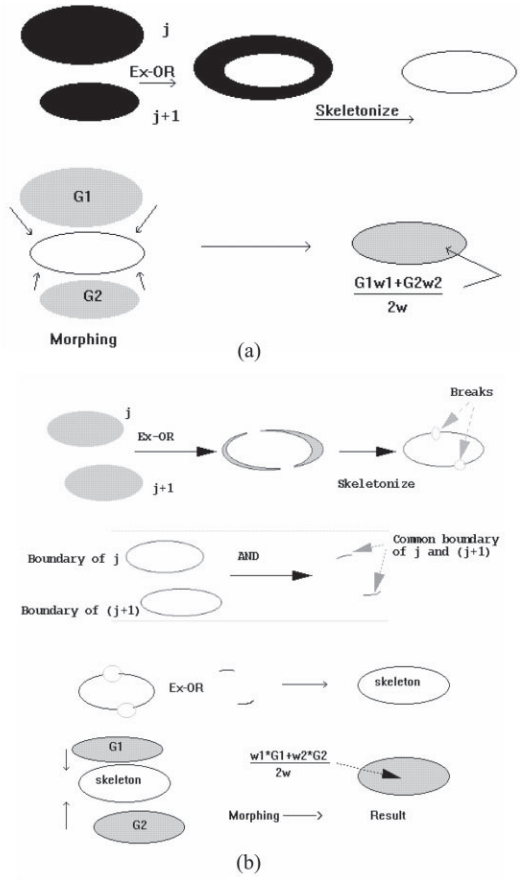

Fig. 6. (a) Diagrammatic representation of interpolation by morphing. (b) Interpolation by morphing when the object shape in the source images are different or when they are laterally shifted.

3.1. Smoothing

The aim is to smooth the highly textural cell chromatin without reducing the sharpness of the boundary features. Simple spatial averaging blurs the cell boundary while smoothing, an undesirable effect. Symmetrical Gaussian smoothing blurs the edges while smoothing, though the influence of far-off voxels on the smoothing is reduced. To reduce the blurring effect on the edges, we have used directional Gaussian filtering. A 5×5 Gaussian filter is subdivided into six directional windows as shown in Fig. 5. The Gaussian-convolved values of the pixels in each directional window are calculated as shown.

The maximum of the convolution values in all the directional windows gives the desired result. If $v(\mathrm{x},\mathrm{y};\theta)$ are calculated in several directions as $v(x, y; \theta) = (1/N_\theta) \sum_{(m,n)\in W_\theta} \sum u(x, y)G(x - m, y - n)$ where $G(x, y) = \exp\{(x^2 + y^2)/2\sigma^2\}$ is a Gaussian filter, N_θ is the total number of pixels present in the directional window W_θ as shown in Fig. 5.

A direction θ^* is found such that $|u(x, y) - v(x, y; \theta^*)|$ is a minimum. Then the output image $v(x, y) \Leftarrow v(x, y, \theta^*)$ is the desired result. The directional Gaussian smoothing technique is applied separately to all the image slices in the image stack.

4. Enhancement of axial resolution

One of the important enhancement steps to be carried out is the improvement of axial resolution of the image stack. Due to anisotropy in the voxel lattice, the direct 3D processing algorithms fail to properly make use of spatial neighbourhood relations. To avoid these errors, and to enhance the qualitative and quantitative accuracy of visualization and analysis, a suitable interpolation process has to be used to increase the axial resolution of the stack. Classical interpolation techniques fall into three categories: contour-, intensity- and shape-based interpolations.

Contour-based interpolation (Boissonat, 1988) takes a set of binary images containing cross-sectional boundaries of the objects and generates a new set of interpolated binary sequence representing the surface of the objects. Since only the contours of the selected features are used in the interpolation process, critical intensity information would be lost. Intensity-based interpolation takes the original voxel intensity values and generates a new set of interpolated voxel intensities. If there is a shape variation in the two source images, this method results in error. This is so because calculation of the interpolated value only takes a limited number of data points and produces a wrong estimation when there is shape variation between two source

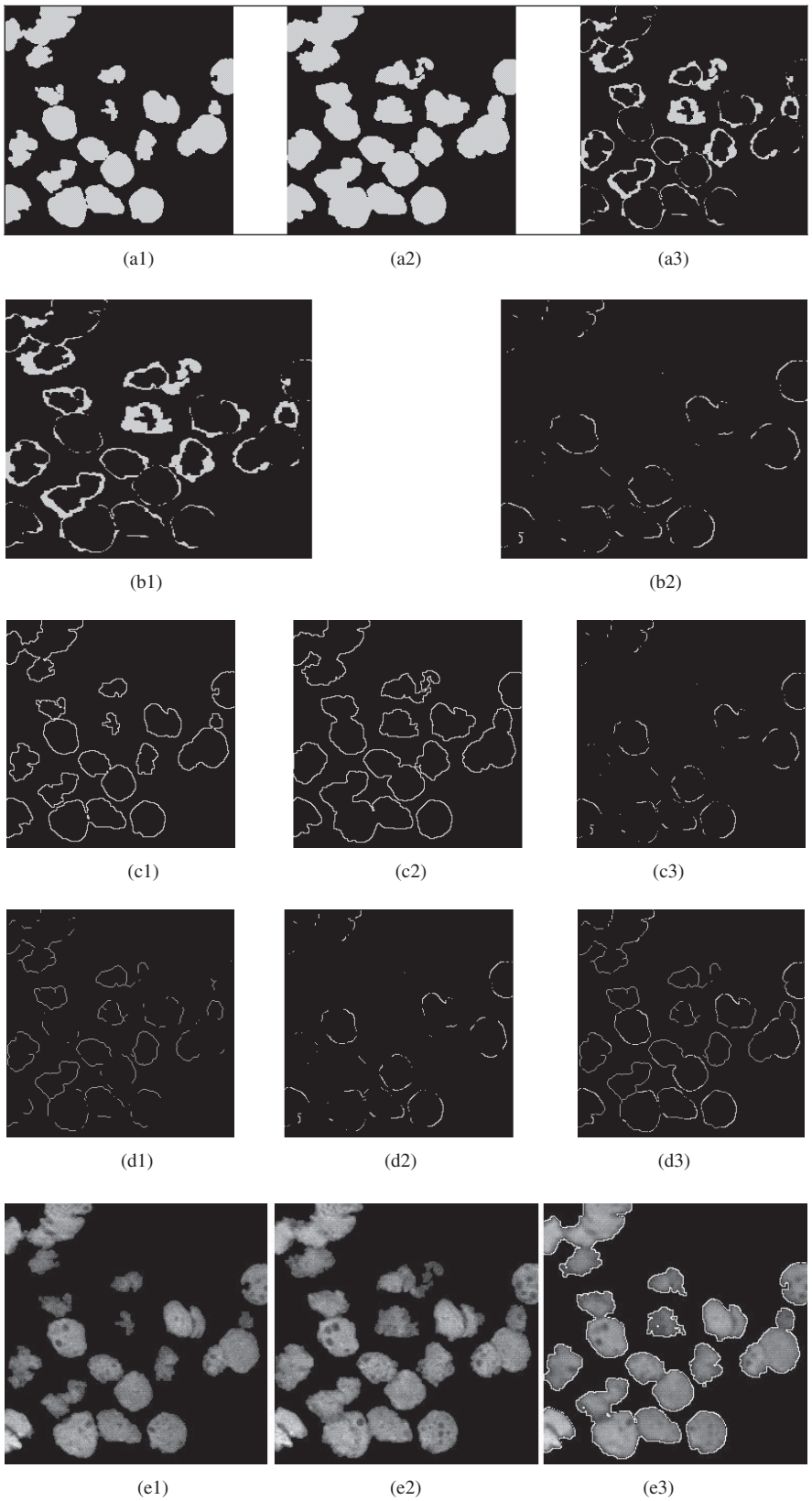

Fig. 7. Result of each step of interpolation by morphing, as applied to two representative image slices. (a) Two-tone version of the source image slices subject to XOR operation; (a1) and (a2) two-tone versions of source images 1 and 2, respectively; and (a3) after XOR operation. (b) After skeletonization of the image in Fig. 7(a3). (c) Result of XOR operation on the boundary of the source images; (c1) and (c2) boundary of source images; and (c3) result of ANDing (c1) and (c2). (d) Result of linking the broken contours; (d1) same as Fig. 7(c1); (d2) same as Fig. 7(c3); (d3) complete contour in the interpolated image slice = (d1) XOR (d2). (e) Two source images (e1) and (e2), (e3) = Result of morphing.

images. Shape-based interpolation (Raya and Udupa, 1990) takes a set of binary images representing cross-sections of objects segmented from the intensity-value data and performs morphological interpolation between shapes and contours. To avoid the errors due to contour- and intensity-based interpolation, we have developed a method where the contours of the objects in the interpolated image slice are first obtained by logical operation over the source images and then using these contour pixels as the control points, the intensity of the pixels within the contour are calculated by morphing two source images. The process is explained below.

Consider the two-tone version of two neighbouring image slices (source images) j and $(j + 1)$, where the object is represented by grey level 1 and the background by 0 as shown in Figs. 6 and 7(a). For creating an image slice in between j and $(j + 1)$, we have to choose some control point in the interpolated image slice towards which the source images are distorted during morphing. It can be argued that if by some means we can get the overall boundary of the objects in the interpolated image slice, we can use these edge pixels as control points and fill the grey level within these boundary points using morphing or a weighted-averaging technique. The overall boundary of the objects in the interpolated image slice can be found by using simple logical operations as follows. The two-tone versions of the neighbouring image slices j and $(j + 1)$ are subject to pixel-to-pixel XOR operation. The resulting image consists of the portion of the object that is common to the objects in both j and $(j + 1)$ image slices. This is shown diagrammatically in Fig. 6. The medial axis of this image gives the boundary of the objects in the interpolated image slice.

If the objects in j and $(j + 1)$ image slices are laterally shifted or there is a strong variation in shape of the objects between two source images, then the resulting medial axis need not be continuous. To join the disconnected boundary, we have applied the following simple operation. The contours of the objects in the two source images are obtained over a two-tone version of the source images j and $(j + 1)$. The common portion of the boundary of the objects in j and $(j + 1)$ image slices are obtained by pixel-to-pixel AND operation of the two boundary maps of the source images. The result of the AND operation is added to the medial axis of the interpolated image slice by the logical OR operation. This results in linking the broken contour. The process is shown diagrammatically in Fig. 6. Fig. 7 shows each interpolation step as applied to a pair of CLSM image slices.

To fill the intensity information within the boundary contour of an interpolated image slice, the window-sliced version of source images j and $(j + 1)$ are distorted towards the position of the contour-based control points in the interpolated image slice. Then, the two deformed images are blended with simple weighted averaging to generate the grey value in the interpolated image slice. Let $G_j = I_{j0}, I_{j1}, I_{j2}, \ldots, I_{jn}$ be the grey value of the object pixels in source image j and $G_{j+1} = I_{j0+1}, I_{j1+1}, I_{j2+1}, \ldots, I_{jn+1}$ be the grey value of the object pixels in source image $(j + 1)$. Then, the grey value of corresponding object pixels in the interpolated image slice is given as $(w_1G_1 + w_2G_2)/2w$ where w_1, w_2 and w are constants that are determined experimentally. In our experiment we have used all the weights as 1, simplifying the method to simple averaging. For the pixels that fall outside the boundary contour in the interpolated image slice, the grey value is given as zero. Since most conspicuous features (to human eyes) in images occur at the places with higher gradient magnitudes, which is also where the contour or boundary point usually lies, using contours as control lines for morphing is very effective. Fig. 7 shows the different intermediate steps of interpolation by morphing between two images.

5. Discussion

The work presented here outlines some simple but efficient techniques based on image processing that can be used to correct and enhance the visual quality of the confocal microscopy images. The algorithms were implemented in IDL and C languages on a SGI IRIX5.3 system. We have developed these techniques as a part of the major project of developing algorithms for quantitative analysis of 3D histopathological images obtained using a confocal microscope (Rodenacker et al., 1997; Umesh Adiga and Chaudhuri, 1999a,b, 2000a,b). It has been said that there is no ideal specimen for imaging. Preparing a specimen to acquire a stack of optical sections is a tedious and fatiguing task, which requires scientific precision to preserve the cellularity and architecture of the tissue from falling apart. So, it is prudent to develop image-processing methods to reduce noise artefacts in the image and to enhance the visual quality rather than attempting to prepare an ideal specimen.

We have applied these image-correction techniques to more than 200 confocal image data sets. It is our belief that the visual quality of the image is improved by our methods. Figs. 2, 3 and 7 give some insight into the results we have obtained. The window-slicing method we have proposed is an automatic-thresholding technique where the local threshold is chosen by a data-driven process. This has the advantage of automation and rejecting the influence of bright patches in far-off places in the image. The directional Gaussian smoothing is an improvement over a simple directional-averaging filter. The intensity-enhancement technique we have adopted is a straightforward one. It serves the purpose of visual enhancement of the objects deep down in the image stack, but, as mentioned earlier, one should find a trade-off between the loss of voxel sensitivity and increase in voxel intensity.

The interpolation method we have proposed is superior to the straightforward contour- or intensity-based methods as it incorporates a priori information in the process of interpolation. The shape of the object in the interpolated image is

defined by the contours obtained by logical operations while the intensity is filled by warping the grey levels of the data points in the source images. The histo-pathological images exhibit large local intensity variations and the intensity-filling process presented here gives more realistic results.

Acknowledgements

We would like to thank the reviewers for their suggestions. Help from scientists of the Institute of Pathology, GSF, Munich, Germany is also acknowledged with thanks. Thanks to Mr U. Garain for constructive discussions while preparing the manuscript.

References

Aubele, M., Zitzelberger, H., Szucs, S., Werner, M., Brasselman, H., Hutzler, P., Rodenacker, K., Lehman, L., Minkus, G., Hofler, H., 1996. Comparative FISH signal analysis of numerical chromosome and abnormalities in 5 μm and 15 μm paraffin embedded tissue sections from prostate carcinoma. Int. J. Histochem. Cell. Biol., 121–126.

Boissonat, J.D., 1988. Shape based reconstruction from planar cross sections. Comput. Vision Graphics Image Process. 44, 1–29.

Jain, A.K., 1995. Fundamentals of Digital Image Processing, Prentice Hall of India Pvt Ltd, New Delhi.

Pawley, J., 1995. Handbook of Biological Confocal Microscopy, Plenum Press, New York.

Raya, S.P., Udupa, J.K., 1990. Shape based interpolation of multidimensional objects. IEEE Trans. Med. Imag. 9, 137–141.

Rigaut, J.P., Carvajal-Gonzalez, S., Vassey, J., 1992. Three-dimensional Cytometry. In: Kriete, A. (Ed.). Visualization in Biomedical Microscopies: 3-D Imaging and Computer Applications, VCH, New York, pp. 205–248.

Rodenacker, K., Aubele, M., Hutzler, P., Umesh Adiga, P.S., 1997. Groping for quantitative 3D image analysis: an approach to quantitative evaluation of fluorescence in situ hybridization in thick tissue sections of prostate carcinoma. Anal. Cell. Pathol. 15, 19–29.

Russ, J.C., 1995. The Image Processing Handbook, CRC Press, London.

Umesh Adiga, P.S., Chaudhuri, B.B., 1999a. An efficient cell segmentation tool for confocal microscopy tissue images for quantitative evaluation of FISH signals. Int. J. Microscopy Res. Techniques 43, 1–20.

Umesh Adiga, P.S., Chaudhuri, B.B., 1999b. Deformable models for segmentation of CLSM images and its application in FISH signal analysis. Int. J. Anal. Cell. Pathol. 18 (4), 211–225.

Umesh Adiga, P.S., Chaudhuri, B.B., 2000a. Region based techniques for segmentation of volumetric histo-pathological images. Comput. Methods Programs Bio-Med. 61 (1), 23–47.

Umesh Adiga, P.S., Chaudhuri, B.B., 2000b. Segmentation and counting of FISH signals in confocal microscopy images. Micron 31 (1), 5–15.